

UNSTEADY AERODYNAMIC OPTIMIZATION OF A THIN ANGULAR AIRFOIL USING CARTESIAN MESH CFD WITH THE LEVEL SET METHOD

Daisuke Sasaki[1], Yuma Chikamoto[1], Yuki Kawamoto[1], Masato Okamoto[2] & Hiroki Nagai[3]

[1]Osaka Metropolitan University, Sakai, Japan
[2]Kanazawa Institute of Technology, Nonoichi, Japan
[3]Institute of Fluid Science, Tohoku University, Sendai, Japan

Abstract

In recent years, research and development of micro-air vehicles (MAVs) has been conducted. One of the demands for MAVs are to increase the operational time, which is realized by improving aerodynamic performance or battery run-time. Because MAVs are small and fly at low speeds, their Reynolds numbers become significantly lower than those of conventional aircraft, typically ranging from 10^3 —10^5. In the low Reynolds number region, viscosity highly affects the flowfield, leading to complicated unsteady flow phenomena and also prevents generating sufficient lift. In this study, unsteady flow analysis based on Cartesian mesh with level set method was introduced directly into aerodynamic optimization using Differential Evolution (DE). Because the converged solution was set as the initial solution of a new design, the computational cost for the new design was shortened. Optimization results by the DE show that the maximum camber position highly affects the formation of laminar separation bubbles and also the time-averaged lift-to-drag ratio.

Keywords: Aerodynamic Optimization, Unsteady Flow, Cartesian Mesh, Low Reynolds Number

1. Introduction

In recent years, Micro Air Vehicles (MAVs) have been used a lot for disaster spots, ecosystemic observation, and topography investigation. Since the full length of the body is on the cm scale, the Reynolds number of MAVs becomes low (10^3–10^5). In the low Reynolds number regime, a characteristic phenomenon known as the laminar separation bubble (LSB) occurs. When the laminar boundary layer separates in low Reynolds number flows, a strong adverse pressure gradient is generated, causing the flow to detach from the airfoil surface. The separated shear layer rapidly transitions to turbulence, and, as a result, the turbulent flow may reattach to the airfoil surface, forming a turbulent boundary layer. This phenomenon, LSB, significantly influences the aerodynamic performance, which implies that accurately capturing the behavior of separation bubbles and similar phenomena is crucial in analyzing the performance of objects in low Reynolds number flows using computational fluid dynamics (CFD).

Biomimetics is an effective tool to design an effective wing at low Reynolds number flow. In particular, dragonflies are considered to have high flying ability, and the corrugated wing section is called the corrugated thin wing section. Y. Yamaguchi et al. computed flow around a corrugated wing and the influence of corrugation or unevenness on flowfields and aerodynamic performance [1]. H. Tang et al. optimized the corrugated wing to maximize the lift-drag ratio by focusing on the wavy airfoils [2]. Through optimization, it was revealed that the shape like the thin arc wing is aerodynamically superior in aerodynamic performance than wavy airfoils. T. Itami et al. reported that the maximum camber position of a thin circular airfoil affects the aerodynamic characteristics through the optimization under Reynolds number of 40000 [3]. As a result, it was found that the maximum camber position affected the vortex structure in the flowfield and the generation position and size of separation bubbles on the airfoil surface.

https://doi.org/10.71945/icas2026_0767

As mentioned in the literature, it has been found that thin airfoil with camber is superior to the thick airfoil in terms of aerodynamic performance in the low Reynolds number range [4]. A further improvement in aerodynamic performance is required for the increase in operational time. One of the promising approaches is to conduct unsteady aerodynamic optimization of thin airfoils to improve aerodynamic performance under low Reynolds number flow. However, an unsteady aerodynamic simulation often requires large computational time for pre-processing (meshing) and flow computation. Particularly, when structured or unstructured mesh are used for CFD evaluation of a new design candidate during the optimization, meshing procedures are generally required.

In this study, Cartesian-mesh CFD with the level set method [5] is used to represent a thin airfoil and to capture the complicated flow phenomena, including LSB. The geometry is represented by the level set method. In addition, a new geometry or a modified geometry is generated by the modification of the level set function. Re-meshing is not required for the procedure, which leads to the reduction of pre-processing time. In addition, the converged original flowfield is used as the initial condition of the deformed geometry to reduce computational time.

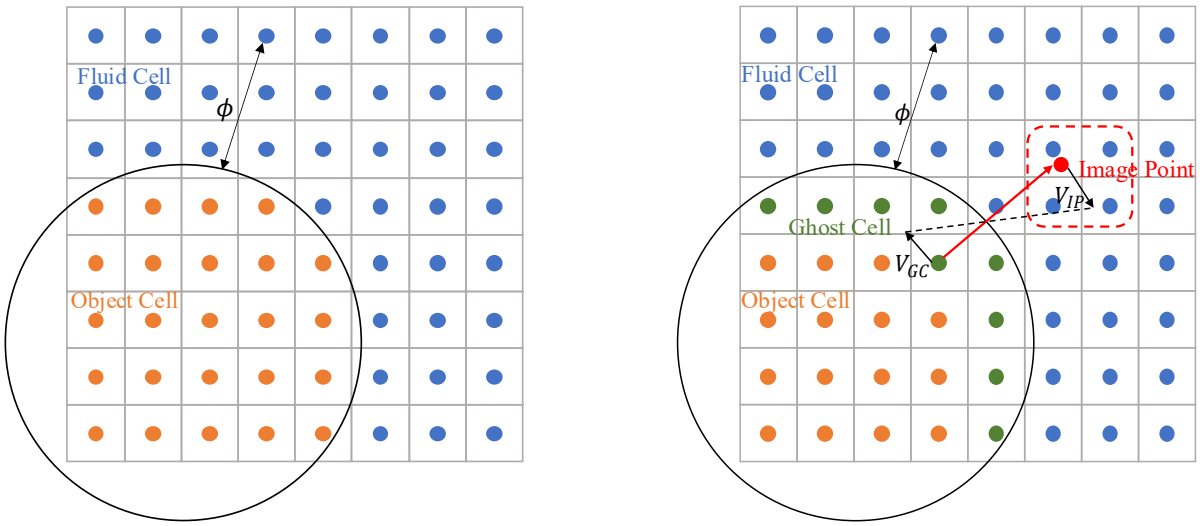
The objective of the study is to apply unsteady aerodynamic optimization with the Cartesian-mesh CFD mentioned above for thin angular airfoil to maximize the time-averaged lift-to-drag ratio. Making use of the advantage of Cartesian mesh with level set function, a new geometry is directly manipulated from the original results. Differential Evolution (DE, [6]) is used for the optimization algorithm to efficiently search the wide design space. The results are also examined to clarify the characteristics of a thin angular airfoil.

2. Methodology

2.1 Flow Solver

A two-dimensional incompressible flow analysis solver for the equally-spaced Cartesian mesh [5] was used to analyze the flow at a Reynolds number of 7000. The governing equations for the two-dimensional model are the incompressible Navier-Stokes equations and the continuity equation. The fractional step method is used to solve the incompressible Navier-Stokes equations. As a discretization method for the convective term of the Navier-Stokes equations, a fifth-order WENO (Weighted Essentially Non-Oscillatory) method is used, while a second-order central difference scheme is used for the viscous term. For the time integration of the convective term, a third-order TVD Runge‑Kutta method is used.

In this study, ghost-cell immersed boundary method combined with the level set method was used to define the shape of the objects. In this method, a level set function $\emptyset$ is assigned to each cell, as shown in Figure 1 (a), which is a signed distance function from the geometry surface. The sign of $\emptyset$ determines the attributes of the computational mesh, where $\emptyset = 0$ represents the interface, and $\emptyset > 0$ and $\emptyset < 0$ represent the fluid and the interior of the object, respectively. In addition, Ghost Cell method is used in immersed boundary method to represent the no-slip condition on the object surface as shown in Figure 1 (b). Ghost Cell is defined as $-2\sqrt{3}\Delta x \leq \phi \leq 0$, and Image Point is defined as $1.45\Delta x$ away from Ghost Cell in normal direction, where Δx is the minimum mesh spacing allocated near the object. Assuming that the velocity gradient is constant between the image point, the Ghost Cell, and the object surface, extrapolate the velocity to the Ghost Cell to represent the object surface. In contrast, the pressure is extrapolated from the Image Point value so that the pressure gradient near the object is zero.



(a) Level set method (b) Ghost cell method

Figure 1 – Immersed boundary method.

2.2 Optimization Method

Differential Evolution (DE) is employed as the optimization method. DE is a kind of evolutionary optimization algorithm like Genetic Algorithm (GA). GA generates new individuals using recombination (crossover) between parent solutions and occasional mutation, while DE generates new individuals using difference vectors between randomly selected individuals, combined with simple crossover and selection. The overview of the concept is sketched in Figure 2. This mechanism makes DE highly effective for continuous optimization. DE also has the advantage of a very simple algorithm with few control parameters. The procedure for DE is as follows:

(1) Evaluate objective function of *N* initial solutions

(2) Choose target vector x_i

(3) Choose base vector x_b and other 2 vectors (x_{r1}, x_{r2}) randomly $(b, r_1, r_2 \neq i)$

(4) Create mutant vector v_i by x_b, x_{r1}, x_{r2}

$$v_i = x_b + F(x_{r1} - x_{r2}) \tag{1}$$

where $F \in [0,2]$ is scale factor or differential weight.

(5) Create trial vector u_i by mixing the target vector and mutant vector

$$u_i = \begin{cases} v_i & \text{if } (\text{rand} \leq C_r \text{ or } j = j_{rand}) \\ x_i & \text{otherwise} \end{cases} \tag{2}$$

where $C_r \in [0,1]$ is the crossover rate and j_{rand} ensures at least one dimension comes from the mutant (prevent generating the same).

(6) Evaluate objective function of trial vector

(7) Compare the objective function of the target vector and the trial vector and select the better vector for the next generation individual (greedy selection).

$$x_i^{NEW} = \begin{cases} u_i & \text{if } f(u_i) \leq f(x_i) \\ x_i & \text{otherwise} \end{cases} \tag{3}$$

(8) Repeat process (2) to (7) for *N* times

(9) Update the generation and start process (2) until the convergent condition satisfies

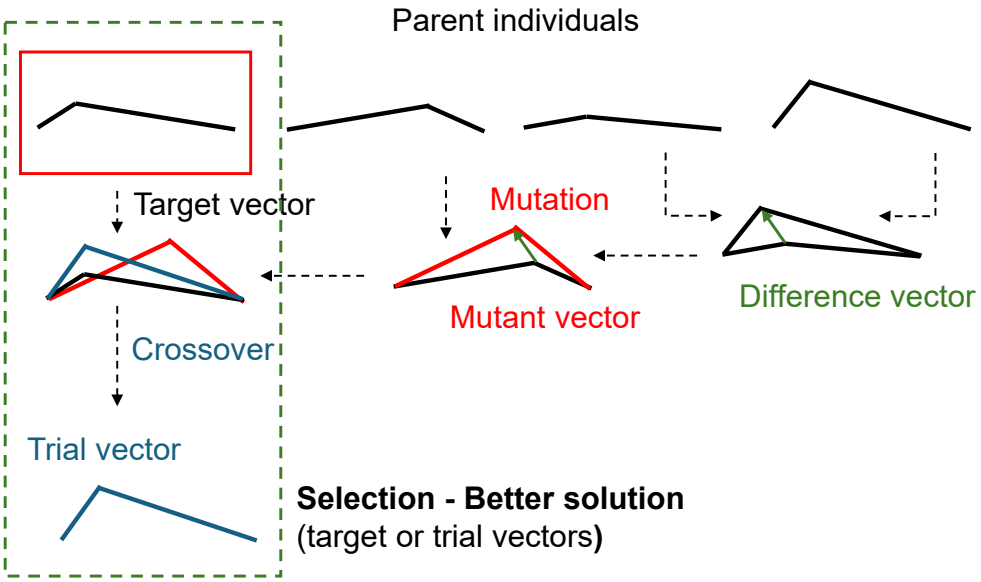


Figure 2 – Generation of a new design candidate by DE.

2.3 Optimization Setup

The optimization target is a thin angular airfoil as shown in Figure 3. The chord length of the airfoil is 0.1 m, the thickness is 0.001 m. The objective of an aerodynamic optimization is to maximize the time-averaged lift-to-drag (L/D) ratio at angle of attack 5 degrees under Reynolds number of 7000. The design variables are the maximum camber location, a/c, and the camber height b/c as appeared in Figure 3. The design range of the maximum camber location is 30 % ≤ a/c ≤ 70 %, and the camber height is 3 % ≤ b/c ≤ 10 %.

The 2D unsteady, incompressible CFD computation on Cartesian mesh without turbulent model is used to capture the complicated flow phenomena of separation and vortices at Reynolds number 7000. It is noted that the 2D unsteady flow analysis is valid to capture the flow phenomena and aerodynamic performance at low angles of attack in Reynolds number 7000 [7]. Figure 4 shows the computational domain for a thin angular airfoil. In the computation, mesh size is set as 2.5×10^{-4} [m], which corresponds to 12.5 million mesh (5000×2500) in total.

In optimization, DE [2] is used as optimizer, where population size is set to 10 and generation is set to 10. The scale factor F is 0.5 and crossover rate C_r is 0.9. Figure 5 shows the flowchart of DE algorithm implemented in the study. Because the geometry is represented by the level set function coupled with the ghost cell method, modified geometry (trial vector) during optimization is represented by updating the level set function. This leads to a reduction of computational time because the generation of mesh for the modified geometry is not necessary. In addition, the previous converged solution was used as initial condition for the computation of modified geometry to accelerate convergence. This is enabled because the same Cartesian mesh is used for the CFD and the level set function only needs to be updated.

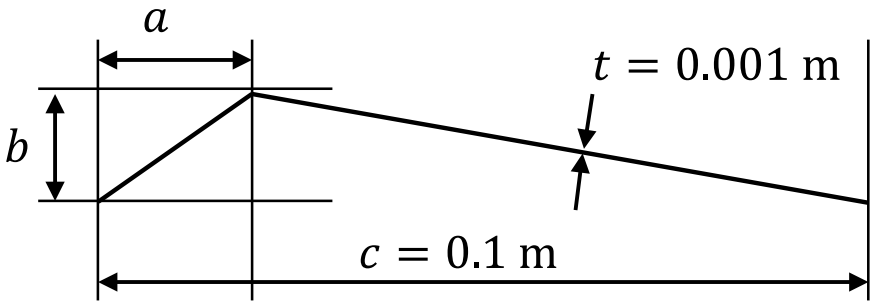


Figure 3 – Definition of a thin angular airfoil.

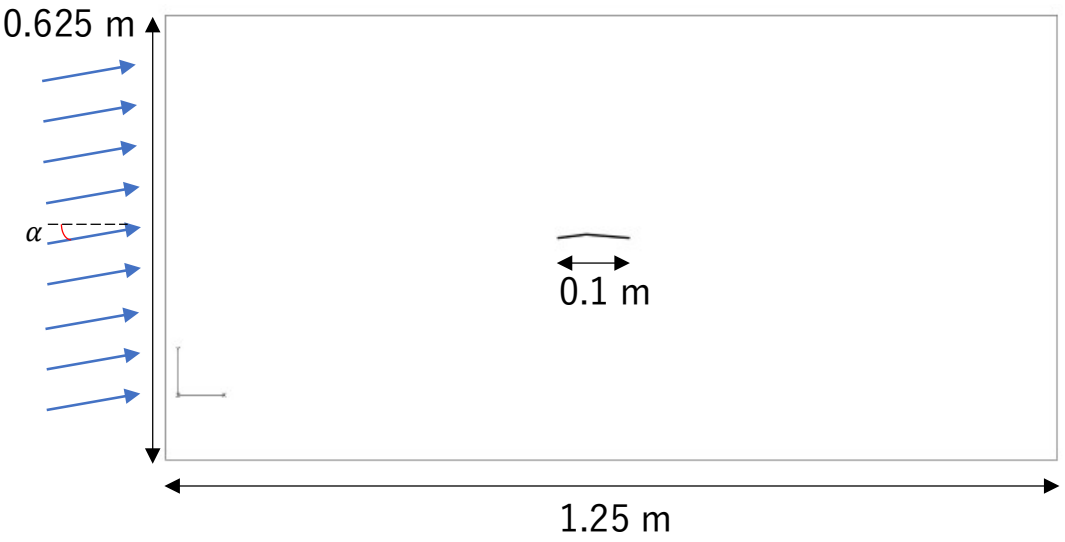


Figure 4 – Computational domain.

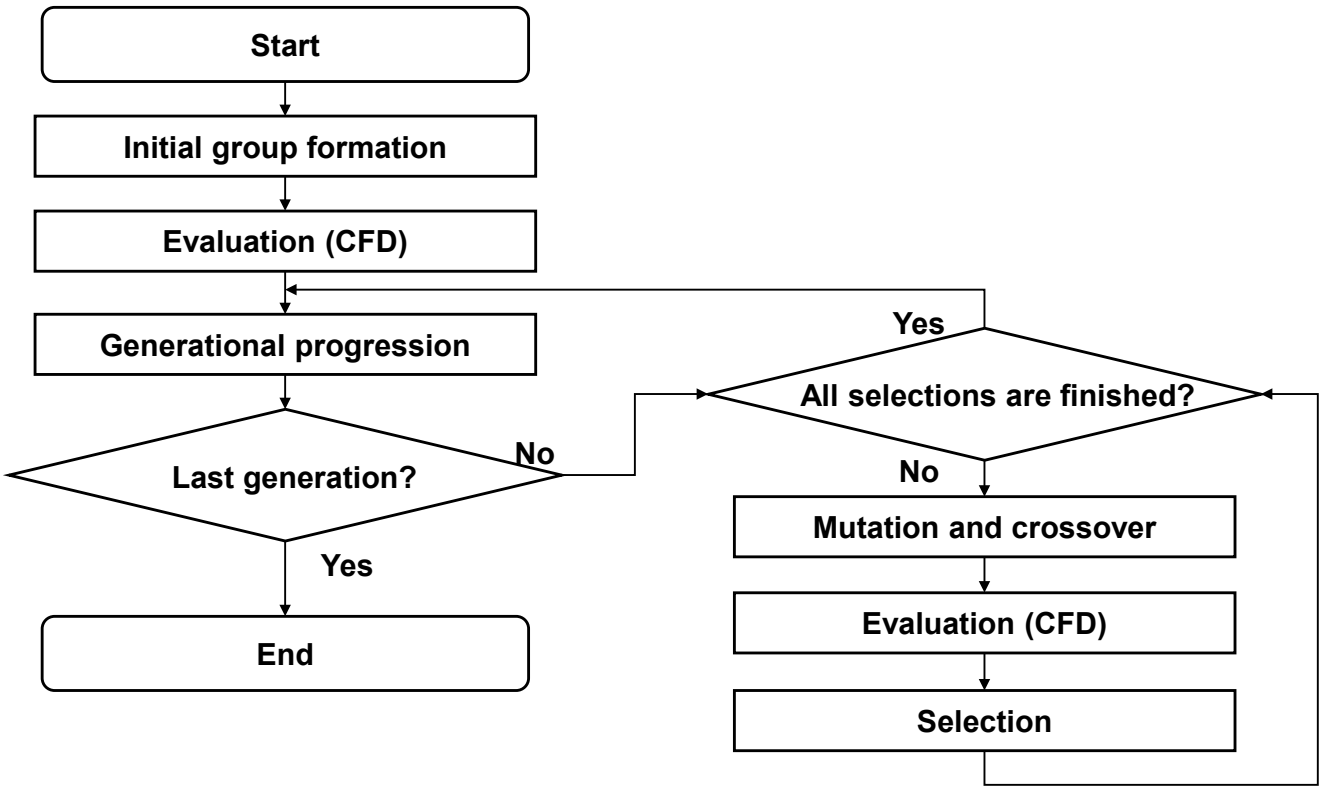


Figure 5 – Flowchart of Differential Evolution.

3. Results

3.1 Strategy

To verify the usefulness of direct modification of geometry within optimization by updating level set function, three optimization cases were conducted. The original converged solution is used as initial solution for a new design candidate for Cases 1 and 2. Instead, all new designs are computed from uniform flowfields for Case 3 (the initial condition is set as uniform velocity field). Because the future

extension of the research is to apply for various angles of attack, initial converged solution is computed at angle of attack 3 degrees not 5 degrees for Case 1. This converged solution is used only for initial generation and the rest is the same as Case 2. This strategy difference is summarized in Table 1.

After optimization for 10 generations, optimal solution was obtained for each case, as shown in Table 2. The optimal solutions of all the cases are quite similar in shape and also objective function. Furthermore, it can be seen from Figure 6 that the population was searched near the optimal solution in all the optimization cases. This is because the population converged near the optimal solution according to the generation update. This reveals that the influence of initial solution on optimization is little. Table 3 shows the number of averaged iterations to convergence. This proves that it is helpful to accelerate the convergence by setting the original converged solution as the initial solution. Case 1 also proves that the converged solution as different angles of attack is also effective compared to Case 3 where uniform flowfields are always set as initial condition. This is a huge benefit to employ Cartesian mesh with the level set method for the unsteady aerodynamic shape optimization to reduce computational time.

Table 1 – Optimization strategy.

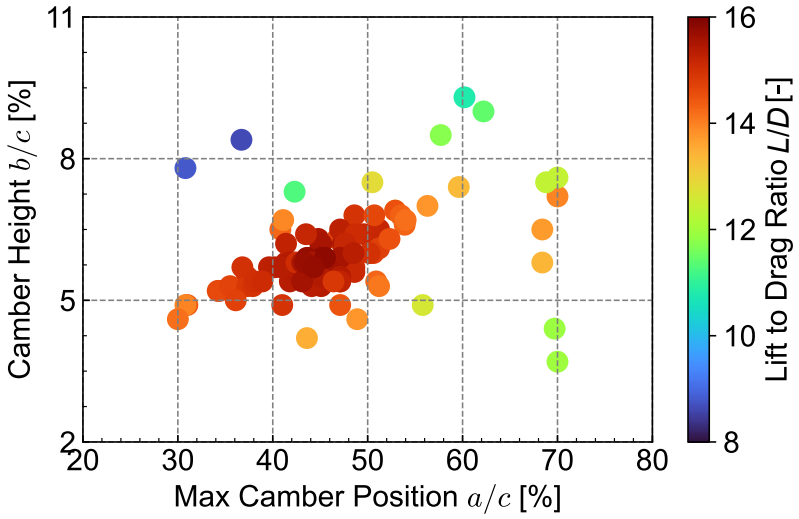
Case	Computational condition of initial solution	Converged solution for initial generation
Case 1	converged solution	converged solution at 3 degrees
Case 2	converged solution	converged solution at 5 degrees
Case 3	uniform flowfield	N/A

Table 2 – Optimal solution of each strategy.

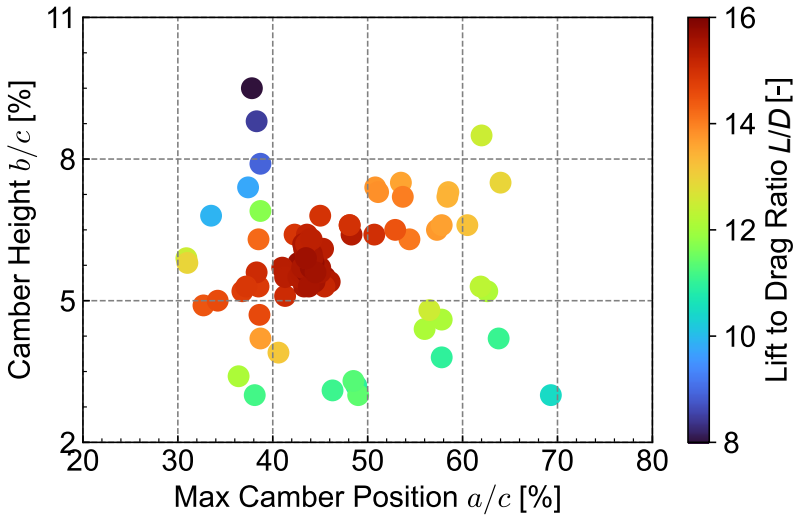
Case	Maximum camber location, a/c [%]	Maximum camber height, b/c [%]	Time-averaged lift-to-drag ratio, L/D [−]
Case 1	45.2	5.8	15.8
Case 2	44.1	5.9	15.7
Case 3	44.7	5.7	15.7

Table 3 – Averaged iteration number for convergence.

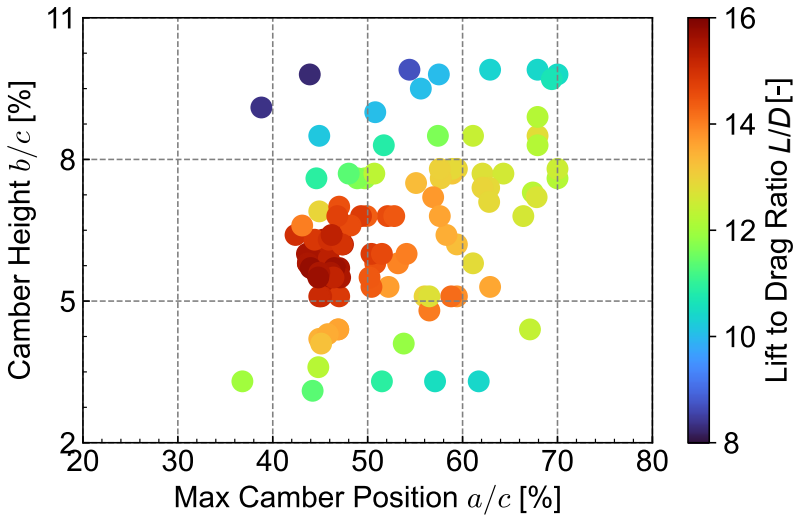
Case	Averaged iterations
Case 1	35700
Case 2	33400
Case 3	51200



(a) Case 1



(b) Case 2



(c) Case 3

Figure 6 – Design candidates with lift-to-drag ratio for different optimization strategies.

3.2 Characteristics of Thin Angular Airfoils

As a result of the three optimizations mentioned in Sec. 3.1, optimized thin angular airfoil was obtained with the L/D of nearly 16. Here, all the solutions are presented on maximized camber position and camber height in Figure 7. The time-averaged lift coefficient, time-averaged drag coefficient, and time-averaged lift-to-drag ratio are also shown in the figure. It shows that the high lift-to-drag ratio is achieved by thin angular airfoils of about 45% maximum camber location and 6% camber height.

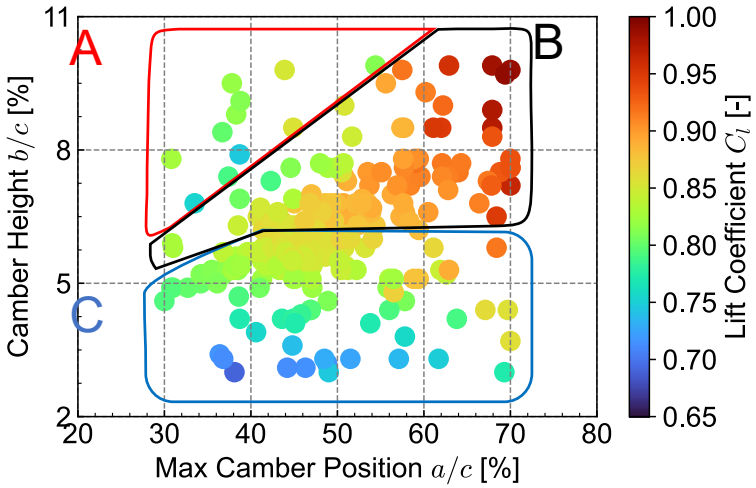
The results were classified into 3 groups: low L/D or high drag (group A), mid L/D or relatively high lift (group B) and relatively higher L/D or lower drag (group C). Three thin angular airfoils from each group are chosen for comparison (airfoils A-C). Airfoils C is the optimal solution with the highest L/D. Figure 8 shows the time-averaged velocity magnitude of the three airfoils. The flowfield of airfoil A is widely laminar without separation at the front of the maximum camber of the airfoil, but a separation vortex forms from the maximum camber position toward the trailing edge, obtained by placing the camber position toward the leading edge and increasing the camber height. It can be seen that the airfoil belonging to group A has a remarkably small lift-drag ratio. In the flowfield of airfoil B, in addition to the generation of separated vortices at the rear as in the airfoil A, a region is observed where the flow is separated from the leading edge of the airfoil and reattached to the airfoil surface. This region is considered to be the laminar separated bubble. A separation vortex is then formed from the camber to the trailing edge. It can be seen that the airfoils belonging to group B have a moderate to high lift-drag ratio.

In the flowfield of airfoil C, the laminar separation bubble is formed at the leading edge of the airfoil, but the separated region at the rear is not confirmed. However, the mean lift-to-drag ratio shows that the same level of lift-to-drag ratio as in group B is obtained. The optimum solution obtained in this study belongs to group C, which is shown in Figure 8 (c).

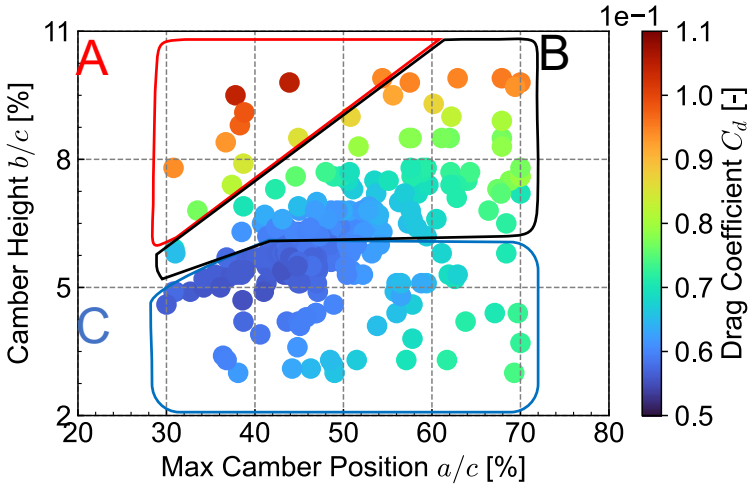
The difference between the flowfields of airfoils A and B is the presence or absence of the separated bubble at the leading edge of the airfoil, which seems to depend on the inflow angle of the flow at the leading edge. From the results shown in Figure 7 (c), it is found that there is a straight line to divide groups A and B, and the angle is about 8.5 degrees. It is more obvious in Figure 9 which is a contour map of L/D generated from all the solutions during the optimization. The figure is created by converting two design variables of maximum camber height and camber location to camber angle and length to the maximum camber. Figure 9 (c) shows that the L/D is largely changed by nearly 8.5 degrees of the camber angle. This means that the relative inflow angle is around 3.5 degrees because the angle of attack is 5 degrees. When the camber angle of an airfoil is smaller than this angle, that is, in group B, the separated flow expands over the upper surface from the leading edge. When the separated flow reattaches to the airfoil surface, a laminar separation bubble is formed, and when the angle is further decreased, the laminar separation bubble is considered to grow larger and longer. On the other hand, when the angle is higher, that is, in Group A, the flow on the upper surface is accelerated, which is considered to prevent separation. However, as the camber angle increases, the suction of the flow at the leading edge increases. The airfoils are designed by shifting the camber position further toward the trailing edge compared to group A. Therefore, this angle is considered to change for any shape and angle of attack. The group C contains an airfoil with separation bubbles forming at the leading edge, obtained by reducing the camber height in comparison to the former two airfoil groups.

Figure 10 shows the time-averaged surface pressure coefficient distribution of the three airfoils. It can be seen from the figure that the negative pressure increases in the region of the separation vortex that appeared at the rear of the airfoils A and B. However, it is considered that pressure drag increases in these shapes because the force acting in the direction perpendicular to the rear is geometrically decomposed into the drag component more than the lift. Similarly, it is considered that the pressure drag increases as the maximum camber position increases in the trailing edge direction and height, because the separation vortex at the trailing edge increases. In the airfoils belonging to group C, the pressure drag increases as the maximum camber position moves toward the trailing edge. It is considered that this is also because the force is geometrically decomposed into the drag component more than the separation vortex at the rear. Therefore, as the front part of the airfoil becomes perpendicular to the flow, the force generated by the separation bubble can become a

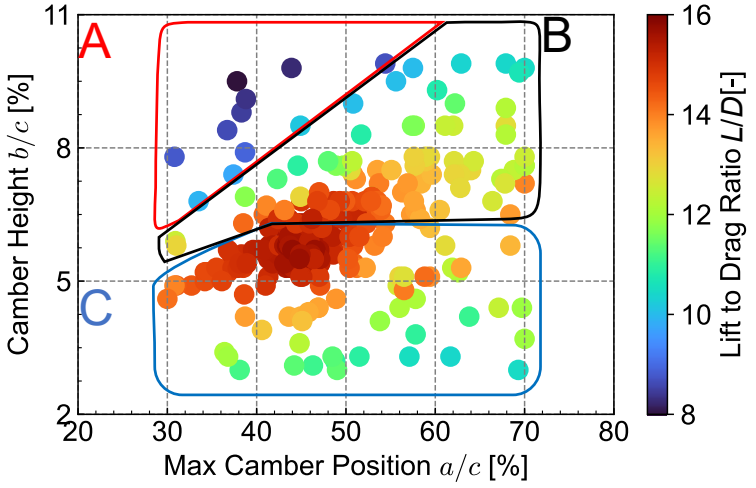
force to cancel the drag. However, this means that the airfoil becomes the shape of A or the shape of C with a low camber height, and such a shape causes a decrease in lift as shown in Figures 7 and 9.



(a) Time-averaged lift coefficient

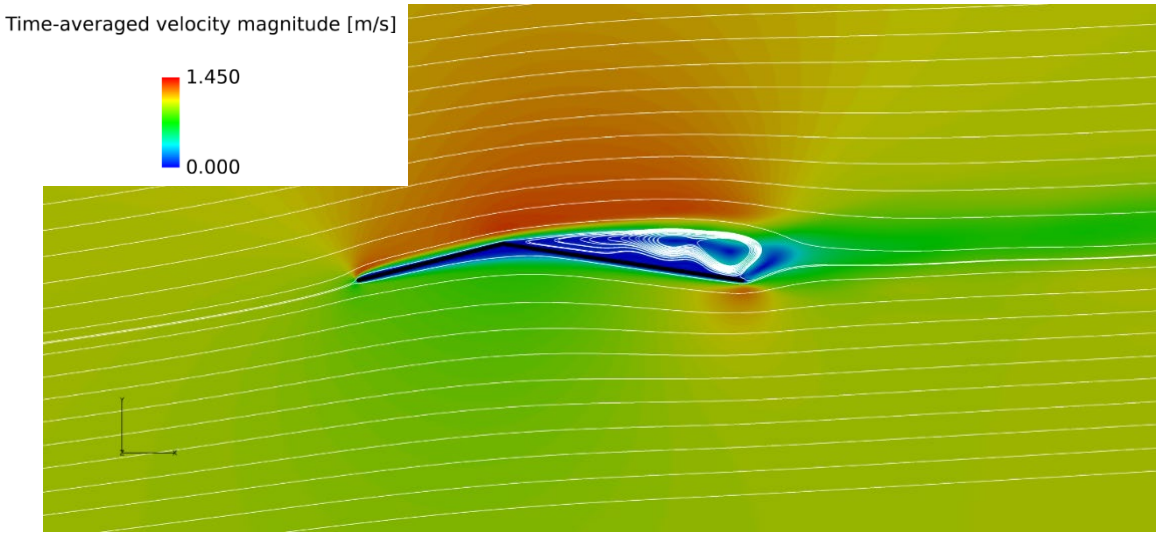


(b) Time-averaged drag coefficient

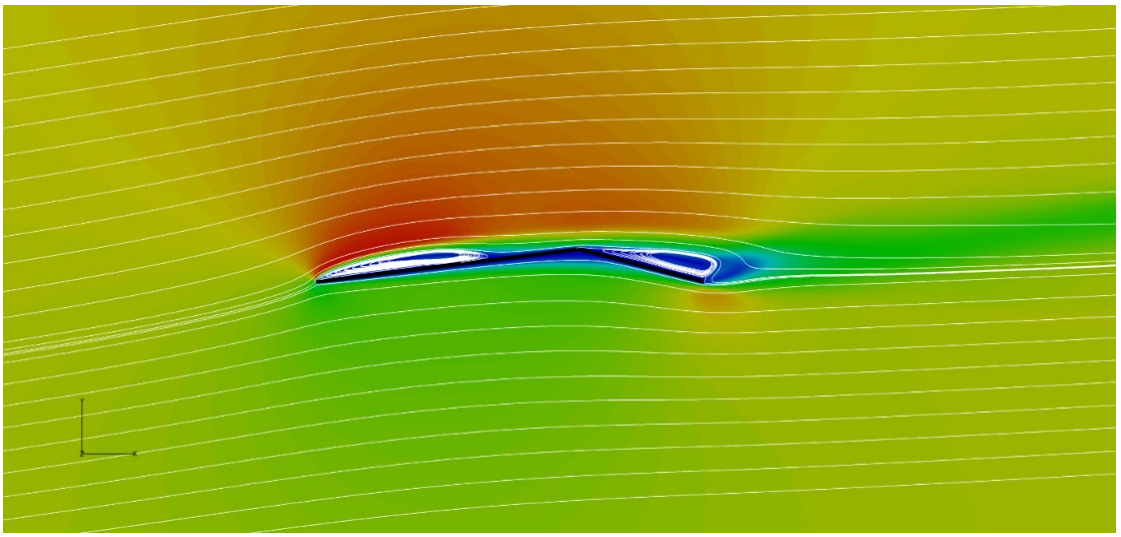


(c) Time-averaged lift-to-drag ratio

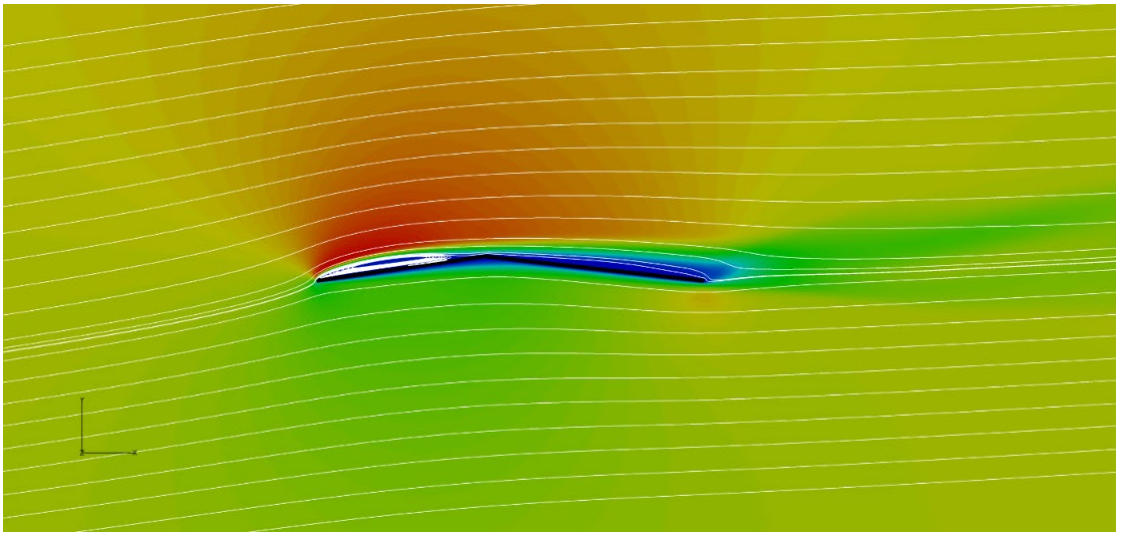
Figure 7 – Aerodynamic performance in design space.



(a) Airfoil A

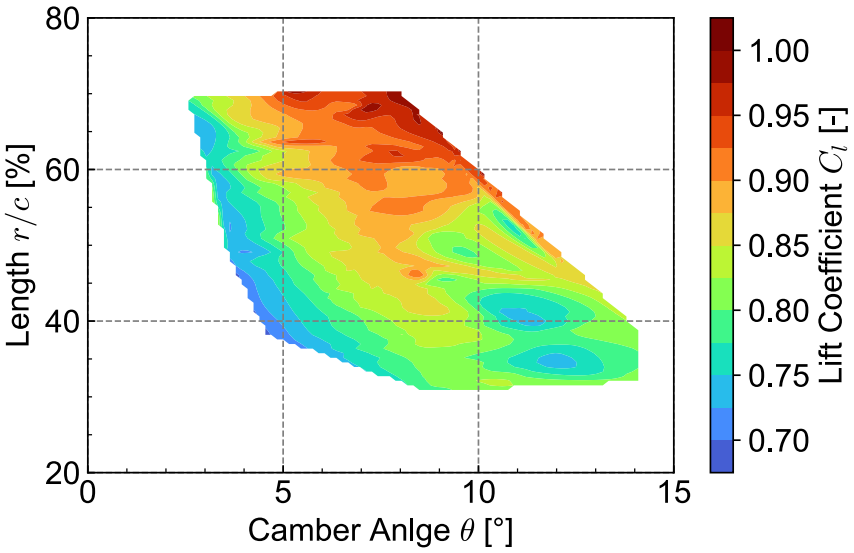


(b) Airfoil B

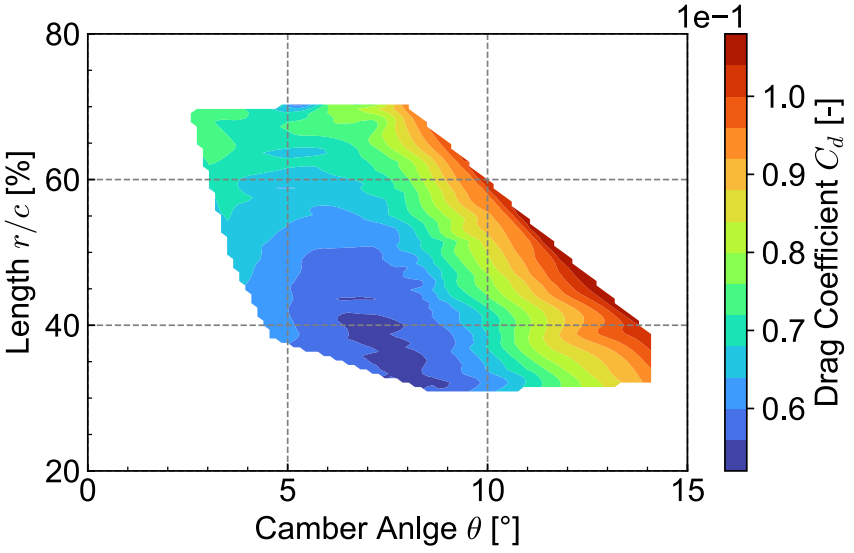


(c) Airfoil C

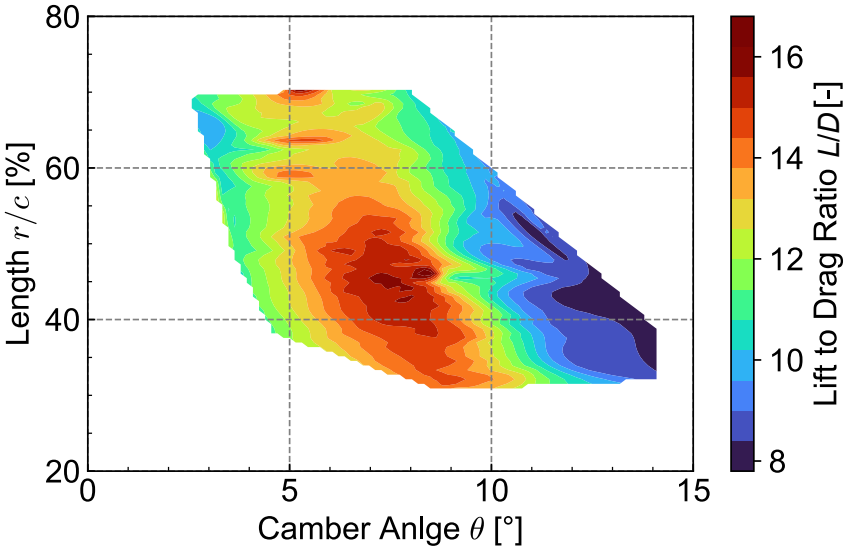
Figure 8 – Time-averaged velocity magnitude of the shapes representing each characteristic.



(a) Time-averaged lift coefficient



(b) Time-averaged drag coefficient



(c) Time-averaged lift-to-drag ratio

Figure 9 – Aerodynamic performance on camber parameters.

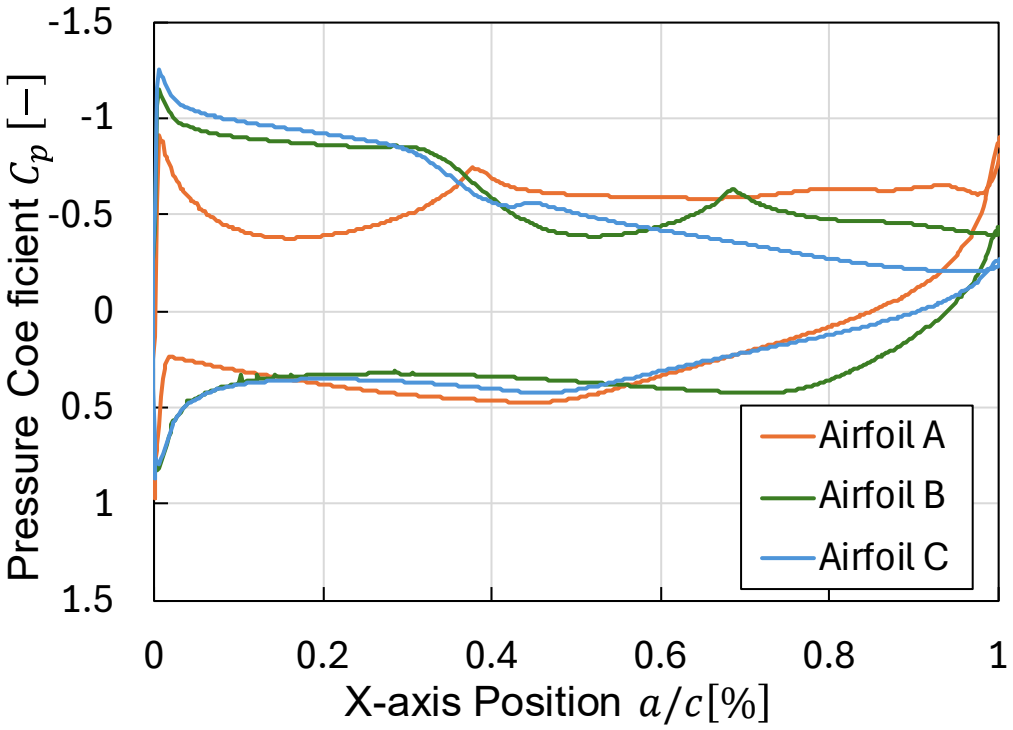


Figure 10 – Time-averaged pressure coefficients of 3 airfoils.

4. Conclusions

In this study, thin angular airfoils were optimized to improve aerodynamic performance using unsteady CFD computation on Cartesian mesh with the level set method. With the advantage of geometry modification based on the level set function and differential evolution, the computational time for unsteady CFD computation for a new design is shortened. The optimal airfoil is designed to form a thin laminar separation bubble, while preventing the flow separation at the camber location. It is concluded that the existence of laminar separation bubble highly affects the aerodynamic performance of the thin angular airfoil, thus the control of camber height and location is essential.

5. Contact Author Email Address

mailto: daisuke.sasaki@omu.ac.jp

6. Copyright Statement

The authors confirm that they, and/or their company or organization, hold copyright on all of the original material included in this paper. The authors also confirm that they have obtained permission, from the copyright holder of any third party material included in this paper, to publish it as part of their paper. The authors confirm that they give permission, or have obtained permission from the copyright holder of this paper, for the publication and distribution of this paper as part of the ICAS proceedings or as individual off-prints from the proceedings.

Acknowledgements

Part of the work was carried out under the Collaborative Research Project of the Institute of Fluid Science, Tohoku University (Project code: J25I040). The analysis was performed using the supercomputers AFINITY II at Advanced Fluid Information Research Center, Institute of Fluid Science, Tohoku University. FieldView was provided by the University Partner Program (UPP) of Tecplot, Inc. to visualize the computational results.

References

[1] Yamaguchi Y, Sasaki D, Okamoto M, Shimoyama K and Obayashi S. Numerical investigation of geometrical corrugation influence to vortex flowfields at low Reynolds number. *Journal of Fluid Science and Technology*, Vol. 19, Issue 3, pp JFST0018, 2019.

[2] Tang H, Lei Y, Li X, Gao K and Li Y. Aerodynamic shape optimization of a wavy airfoil for ultra-Low Reynolds number regime in gliding flight. *Energies*, Vol. 13, No. 467, pp 1-27, 2020.

[3] Itami T, Otake T, Muramatsu A and Motohashi T. Influence of maximum camber position on the aerodynamic characteristics of contact circular arc airfoil at low Reynolds number. *Proceedings of 43rd Fluid Dynamics / Aerospace Numerical Simulation Symposium 2011*, Tokyo, 2011. (in Japanese)

[4] Takeda S and Okamoto M. Aerodynamic characteristics of comb wing at very low Reynolds numbers. *Japan Society for Aeronautical and Space Sciences*, Vol. 70, No. 2, pp 40-47, 2022. (in Japanese)

[5] Osaki H, Sasaki D, Kawamoto Y and Okamoto M. The effects of installing protuberances on a flat plate at low Reynolds numbers. *International Journal of Computational Fluid Dynamics*, Vol.38, No.6-7, pp 488, 2024.

[6] Storn R and Price K. Differential Evolution – a simple and efficient heuristic for global optimization over continuous spaces. *Journal of Global Optimization*, Vol. 11, pp 341–359, 1997.

[7] Takase T, Sasaki D and Okamoto M. Aerodynamic study of a circular arc airfoil at low Reynolds numbers using Cartesian mesh CFD. *International Journal of Computational Fluid Dynamics*, Vol.17, No.3, pp JFST0007, 2022.